The effects of process conditions on the plasma characteristic in radio-frequency capacitively coupled $SiH_4/NH_3/N_2$ plasmas: Two-dimensional simulations*

Liu Xiang-Mei(刘相梅)[a], Song Yuan-Hong(宋远红)[b], Jiang Wei(姜 巍)[a], and Yi Lin(易 林)[a]†

[a] *School of Physics, Huazhong University of Science and Technology, Wuhan* 430074, *China*
[b] *School of Physics and Optoelectronic Technology, Dalian University of Technology, Dalian* 116024, *China*

(Received 16 July 2012; revised manuscript received 18 September 2012)

A two-dimensional (2D) fluid model is presented to study the behavior of silicon plasma mixed with SiH_4, N_2, and NH_3 in a radio-frequency capacitively coupled plasma (CCP) reactor. The plasma–wall interaction (including the deposition) is modeled by using surface reaction coefficients. In the present paper we try to identify, by numerical simulations, the effect of variations of the process parameters on the plasma properties. It is found from our simulations that by increasing the gas pressure and the discharge gap, the electron density profile shape changes continuously from an edge-high to a center-high, thus the thin films become more uniform. Moreover, as the N_2/NH_3 ratio increases from 6/13 to 10/9, the hydrogen content can be significantly decreased, without decreasing the electron density significantly.

Keywords: capacitively coupled plasma, process conditions effects, $SiH_4/NH_3/N_2$ discharges

PACS: 52.65.–y, 52.25.–b, 52.80.Pi **DOI:** 10.1088/1674-1056/22/4/045204

1. Introduction

Capacitively coupled plasma has been widely used for etching and deposition. Due their the high thermal stability, chemical inertness, extreme hardness, and good dielectric properties,[1,2] silicon nitride (Si_3N_4) thin films have been extensively used in the fabrication of microelectronic devices as passivation and mechanical protective layers,[3,4] mask layers,[5] and dielectric materials.[6] Conventionally, high-quality silicon–nitride thin films are mainly deposited at low temperatures (below 400 °C) by using the plasma enhanced chemical vapor deposition (PECVD) method. In many cases, the mixtures of silane with ammonia are used for deposition in 13.56-MHz radio-frequency (RF) plasma.[7] NH_3 discharges produce fast growth rates and films with good conformality. However, the films produced in this way typically contain 10 at%–30 at% bonded hydrogen impurity in the form of N–H and Si–H bonding groups, which occasionally cause the degradation of device characteristics.[8] Therefore, in this paper, the mixtures of silane, ammonia, and nitrogen are used for the Si_3N_4 thin films deposition in 13.56-MHz RF plasma, as the bonded hydrogen impurity can be reduced with the use of molecular nitrogen.

Plasma processing is a key fabrication step, especially for the deposition of Si_3N_4 thin films. To optimize parameters of the equipment and processes during the plasma discharge, an entire understanding of various species densities, like electrons, ions, molecules, radicals, and their behaviors are always expected. Accordingly, a considerable number of detailed investigations have been carried out on the characterization of silicon–nitride films by employing a variety of techniques for over two decades. By using numerical simulations and experimental measurements, Kushner and Goto *et al*.[9,10] studied the remote PECVD for the deposition of silicon–nitride films, and found that Si–N bonds in the film were increased by eliminating the charged species, and the flux of radicals to the substrate can be controlled by flow rates and geometries, but some approximations to simplify the model are used. Nowling[11] studied the silicon–nitride films properties deposited from N_2/SiH_4 gas mixtures, and the results show that gas-phase reactions between nitrogen atoms and silane play an important role in the reaction mechanism. Recently, by using the finite boxes method, Bavafa[12] reported a detail description of the characteristics of silicon–nitride film from silane diluted in ammonia in an arbitrary configuration of a capacitively coupled PECVD reactor. However, despite the intensive investigation of earlier studies, one important aspect has practically not been covered so far, the influence of the process conditions on the properties of silicon–nitride film in $SiH_4/N_2/NH_3$ discharges. Therefore, we report here a systematic research for $SiH_4/N_2/NH_3$ discharges, with the main emphasis on the influence of gas pressure and gas mixture composition on the films properties, especially considering the electrode sizes change.

In this article, the behavior of the silicon–nitride layer in a radio-frequency capacitively coupled $SiH_4/N_2/NH_3$ dis-

*Project supported by the China Postdoctoral Science Foundation (Grant No. 2012M511603), the National Natural Science Foundation of China (Grant Nos. 11105057 and 10775025), the Natural Science Foundation of Hubei Province of China (Grant No. 2007ABA035), and the Program for New Century Excellent Talents in University of China (Grant No. NCET-08-0073).

†Corresponding author. E-mail: yilin@mail.hust.edu.cn

© 2013 Chinese Physical Society and IOP Publishing Ltd

charge is investigated by employing a two-dimensional self-consistent fluid dynamic model. Since the geometry of a reactor can affect the plasma properties, the domain adopted in the simulation is an arbitrary configuration of a capacitively coupled PECVD reactor, and the effect of electrode sizes is investigated. To the best of our knowledge, radicals have great influences on the deposition process, thus a few studies have focused on the role of different radicals. Compared with previous work, we focus our attention on the influence of gas pressure, electrode sizes, and gas mixture composition on the uniformity of electron density. Moreover, the absolute profiles of electron density, electron temperature, major positive ions, and radical densities are also described.

The outline of this article is as follows: in Section 2 we describe the fluid model for the silicon–nitride (Si_3N_4) thin films deposition, whereas the simulation results of process condition effect on the plasma characteristic in $SiH_4/N_2/NH_3$ discharge are presented in Section 3. Conclusions are presented in Section 4.

2. Theoretical model

The fluid model employed in this paper is based on the iterative and time-dependent solution of the continuity and momentum equations for the electrons, ions, and neutral particles.

The main aspects of the fluid model, including the variations of density and flux for different species j (electrons, positive ions, negative ions, and neutrals), are as follows[13,14]

$$\frac{\partial n_j}{\partial t} + \nabla \cdot \boldsymbol{\Gamma}_j = S_j, \tag{1}$$

$$\boldsymbol{\Gamma}_j = \mu_j n_j \boldsymbol{E} - D_j \nabla n_j, \tag{2}$$

where n_j and $\boldsymbol{\Gamma}_j$ are the density and flux of particle j, respectively, and S_j represents the different sources and sink terms of corresponding particles j by electron impact collisions with neutrals and/or by chemical reactions, μ_j is the mobility and D_j is the diffusion coefficients. For neutral particles, the mobility term equals zero. As in Eq. (2), the drift-diffusion approximation assumes that a charged particle reacts instantaneously to a change of the electric field. However, with much larger mass than electrons, ions cannot follow the instantaneous electric field in the discharge area. Thus, an effective electric field $\boldsymbol{E}_{\mathrm{eff},i}$ is introduced to compensate the inertia effects originating from their lower momentum transfer frequency, which can be given by

$$\frac{\partial \boldsymbol{E}_{\mathrm{eff},i}}{\partial t} = \frac{e}{\mu_i m_i}(\boldsymbol{E} - \boldsymbol{E}_{\mathrm{eff},i}). \tag{3}$$

The electric field $\boldsymbol{E}$ and the potential V are calculated using the Poisson equation

$$\nabla^2 V = -\frac{e}{\varepsilon_0}\left(\sum n_+ - \sum n_- - n_{\mathrm{e}}\right), \quad \boldsymbol{E} = -\nabla V, \tag{4}$$

where n_+, n_-, n_{e} represent the positive ions, negative ions, and electron densities, respectively, and ε_0 is the vacuum dielectric constant. The electron temperature T_{e} is calculated self-consistently from the second moment of the Boltzmann equation

$$\frac{\partial(\frac{3}{2}n_{\mathrm{e}}T_{\mathrm{e}})}{\partial t} + \nabla \cdot \boldsymbol{\Gamma}_{\mathrm{w}} = -e\boldsymbol{\Gamma}_{\mathrm{e}} \cdot \boldsymbol{E} + S_{\mathrm{w}},$$

$$\boldsymbol{\Gamma}_{\mathrm{w}} = \frac{5}{2}T_{\mathrm{e}}\boldsymbol{\Gamma}_{\mathrm{e}} - \frac{5}{2}D_{\mathrm{e}}n_{\mathrm{e}}\nabla T_{\mathrm{e}}. \tag{5}$$

$\boldsymbol{\Gamma}_{\mathrm{w}}$ is the electron energy density flux, and S_{w} represents the loss of electron energy due to electron impact collisions, D_{e} and μ_{e} express the electron diffusion coefficient and mobility which meet the Einstein relationship. No energy balance is included for the ions and neutrals, since they are assumed to have the local gas temperature.

To obtain the reaction rate coefficients of every electron–neutral collision, as well as the electron mobility and the diffusion coefficients, which are as a function of the average electron energy, a separate electron energy distribution function (EEDF) module is incorporated to compute the EEDF from the Boltzmann equation in the two-term approximation.

Table 1. Neutral–neutral reactions considered in the model and corresponding reaction rate coefficients.

Reaction	Reaction rate	Reference
$H + SiH_4 \rightarrow H_2 + SiH_3$	3.2×10^{-12}	[16]
$H + Si_2H_6 \rightarrow SiH_3 + SiH_4$	2.7×10^{-12}	[16]
$SiH_2 + SiH_4 \rightarrow Si_2H_6$	6.7×10^{-12}	[16]
$SiH_3 + SiH_3 \rightarrow SiH_2 + SiH_4$	1.5×10^{-10}	[16]
$NH_2 + H \rightarrow NH_3$	10^{-13}	[16]
$NH_2 + NH_2 \rightarrow NH + NH_3$	1.4×10^{-12}	[16]
$NH + SiH_4 \rightarrow H_2 + HSi(NH_2)$	10^{-11}	[16]
$NH_2 + SiH_3 \rightarrow H_2 + HSi(NH_2)$	7.8×10^{-11}	[16]
$NH_2 + SiH_3 \rightarrow NH_3 + SiH_2$	2.1×10^{-11}	[16]
$NH_2 + HSi(NH_2) \rightarrow HSi(NH_2)_2$	10^{-10}	[16]
$H + HSi(NH_2) \rightarrow H_2Si(NH_2)$	3×10^{-10}	[16]
$H + H_2Si(NH_2) \rightarrow HSi(NH_2) + H_2$	3×10^{-10}	[16]
$H + H_2Si(NH_2) \rightarrow SiH_2 + NH_3$	3.5×10^{-11}	[16]
$NH_2 + H_2Si(NH_2) \rightarrow Si(NH_2)_2 + H_2$	9.8×10^{-11}	[16]
$H + Si(NH_2)_2 \rightarrow HSi(NH_2)_2$	3×10^{-10}	[16]
$H + HSi(NH_2)_2 \rightarrow Si(NH_2)_2 + H_2$	3×10^{-10}	[16]
$H + HSi(NH_2)_2 \rightarrow Si(NH_2)_2 + NH_3$	3.3×10^{-11}	[16]
$H + H_2Si(NH_2) \rightarrow H_3Si(NH_2)$	2×10^{-13}	[16]
$NH_2 + Si(NH_2)_2 \rightarrow HSi(NH_2)_3$	10^{-10}	[16]
$H + HSi(NH_2)_2 \rightarrow H_2Si(NH_2)_2$	2.5×10^{-12}	[16]
$NH_2 + HSi(NH_2)_2 \rightarrow HSi(NH_2)_3$	4.2×10^{-11}	[16]
$H + Si(NH_2)_3 \rightarrow HSi(NH_2)_3$	3×10^{-10}	[16]

In this paper, a total of 32 different species j (electrons, ions, neutrals, and radicals) are taken into account, which are: SiH_4, NH_3, N_2, H_2, Si_2H_6, $SiH_4^{(1-3)}$, $SiH_4^{(2-4)}$, SiH_3, SiH_2, $H_2Si(NH_2)$, N, H, NH, NH_2, $Si(NH_2)_3$, Si_2H_5, Si_2H_4, $HSi(NH_2)$, $Si(NH_2)_2$, $HSi(NH_2)_2$, $HSi(NH_2)_3$, SiH_3^+, SiH_3^-, SiH_2^-, $Si_2H_4^+$, NH_3^+, H_2^+, NH_4^+, $Si_2H_5^-$, N_2^+, NH_2^+, e. It is worth mentioning that, in addition to silane ground state

molecules, vibrationally excited silane molecules ($SiH_4^{(1-3)}$ and $SiH_4^{(2-4)}$), formed by electron impact collision on the ground state silane, are also considered, since these molecules carry sufficient internal energy to overcome the barriers in endothermal reactions.[15] Moreover, more than 100 reactions comprising electron impact reactions with silane, nitrogen, ammonia, and hydrogen molecules, neutral–neutral reactions, and ion–neutral reactions are included. The gas phase and surface mechanisms which are finally selected to represent the major reactions in the deposition process are presented in Table 1. More details on the complete chemical kinetic scheme can be found in Refs. [12], [13], and [17].

2.1. Diffusion coefficient and mobility

The electron transport coefficients (mobility and diffusion coefficients) are calculated using a two-term Boltzmann solver for the electron energy distribution function, whereas the collision cross sections needed are taken from Refs. [17]– [19]. For neutral particles, the diffusion coefficients D_{ij} ($m^2{\cdot}s^{-1}$) of species j in every background gas i (N_2, NH_3, SiH_4, H_2, Si_2H_6) are calculated using the equations described in Refs. [19] and [20]

$$D_{ij} = \frac{3}{16}\frac{k_B T_{gas}}{P_{tot}}\frac{(2\pi k_B T_{gas}/m_{ij})^{1/2}}{\pi\sigma_{ij}^2\Omega_D(\Psi)}, \tag{6}$$

where k_B and T_{gas} are the Boltzmann constant and gas temperature, P_{tot} is the total gas pressure, m_{ij} is the reduced mass. The binary collision diameter $\sigma_{ij} = (\sigma_i + \sigma_j)/2$ and diffusion collision integral $\Omega_D(\Psi)$ is described by

$$\Omega_D(\Psi) = \frac{A}{\Psi^B} + \frac{C}{e^{D\Psi}} + \frac{E}{e^{F\Psi}} + \frac{G}{e^{H\Psi}}, \tag{7}$$

$\Psi = T_{gas}/\varepsilon_{ij}$, $\varepsilon_{ij} = (\varepsilon_i \times \varepsilon_j)^{0.5}$, $A = 1.06036$, $B = 0.15610$, $C = 0.19300$, $D = 0.47635$, $E = 1.03587$, $F = 1.52996$, $G = 1.76464$, $H = 3.89411$. The Lennard–Jones parameters ε_j and σ_j are illustrated in Table 2. Then, by using the Blancs law, the diffusion coefficient D_j of species j in the gas mixture can be calculated,

$$\frac{P_{tot}}{D_j} = \sum_i \frac{P_i}{D_{ij}}. \tag{8}$$

For ions, the mobility μ_{ij} of ion j in background neutral i (in $m^2{\cdot}s^{-1}{\cdot}V^{-1}$) can be calculated from the low-electric-field Langevin mobility expression,[19,20]

$$\mu_{ij} = 0.514 m_{ij}^{-0.5}\alpha_i^{-0.5}\frac{T_{gas}}{P_{tot}}, \tag{9}$$

where α_i is the polarizability of gas molecule i given in Table 2. And then, also by using Blancs law, we can get the ion mobility μ_i in the background gases, as well as the diffusion coefficient D_i by the Einstein relationship.

Table 2. Polarizability of gas molecule and Lennard–Jones parameters.

Particle	σ/Å	(ε/k_B)/K	α/Å^3
NH_3	2.92	481.0	2.31
N_2	3.526	139.2	1.74
SiH_4	4.084	207.6	4.62
Si_2H_6	4.42	230.0	8.47
H_2	2.827	59.7	0.805
NH_2	2.65	80.0	
NH	2.65	80.0	
H	2.5	30.0	
SiH_3	3.943	170.3	
SiH_2	3.803	133.1	
Si_2H_5	4.714	306.9	
$H_2Si(NH_2)$	4.45	351.5	

2.2. Boundary conditions

A schematic diagram of the arbitrary configuration of a radio-frequency capacitively coupled plasma reactor is shown in Fig. 1, where the locations of two electrodes in Z direction and R direction are marked as $z1$, $r1$, $z2$, $r2$ and $z0$, $r0$. It should be noted that the thicknesses of two electrodes are taken into account in this simulation. The size of upper electrode is 0.5 cm, while the size of bottom electrode is 1.5 cm. Moreover, the upper electrode is driven by a radio-frequency source, while both lower electrode and sidewall are grounded. If a difference between the positive and negative fluxes is generated towards the powered electrode, a dc current could be created. To take this effect into account, a dc bias voltage is added to the boundary conditions of the potential in the model. This dc bias voltage is calculated self-consistently and adapted over the succeeding RF cycles until the fluxes of the ions and electrons, averaged over one RF cycle, are of equal magnitude. Thus, a potential will be created at the electrodes that causes the dc current to drop to zero. The potential V at the electrodes could be written as

$$V = 0, \quad 0 \le z \le z1, \quad 0 \le r \le r1, \tag{10}$$

$$V = V_0 \sin(2\pi f t) + V_{dc}, \quad z2 < z \le z0, \quad r2 < r \le r1. \tag{11}$$

In the open region, the applied voltage is given by linearly interpolating between $r = r1$ and the wall, and between $r = 0$ and $r = r2$. At the symmetric axis, we have set $\nabla V = 0$.

The boundary conditions for the differential equations specified are as follows:[21] the electron flux at the electrodes, walls, and the open region is given by $\Gamma_e = \frac{1}{4} n_e \upsilon_{th,e}(1-\Theta)$ with the average thermal velocity $\upsilon_{th,e} = \sqrt{8T_e/\pi m_e}$, the electron reflection coefficient $\Theta = 0.25$, and the electron energy flux $\Gamma_w = \frac{5}{2} T_e \Gamma_e$, while the secondary electron emission is neglected now. The negative ion flux at the electrodes, walls, and the open region is $\Gamma_- = \frac{1}{4} n_- \upsilon_{th,i}$, and the positive ion flux is continuous at the above boundary $\partial\Gamma_+/\partial x = 0$. For neutral

particles, the flux at the walls is

$$\Gamma_n = \frac{s_i}{2(2-s_i)} n_n \upsilon_{\rm th}.$$

Here, the sticking probability of neutrals $s_i = \beta_i - \gamma_i$, β_i is the surface reaction coefficients specifying the probability that the neutral i reacts at the surface and γ_i is the recombination probability defined as the probability that a neutral reacts on the surface, the sticking probabilities are obtained from Ref. [12].

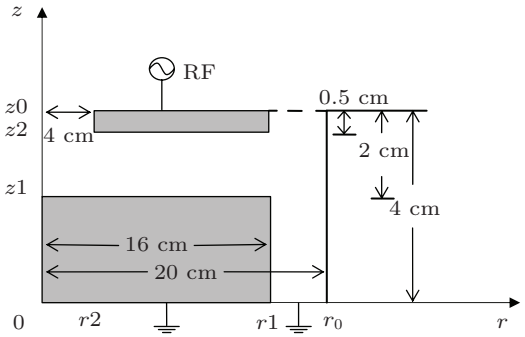


Fig. 1. Schematic diagram of the RF capacitively coupled PECVD reactor shape.

On the other hand, the symmetry at the axial of the reactor implies that the radial components of the particle flux, the electron-energy flux and the RF electric field are equal to zero,

$$\Gamma_j(r=0) = 0, \quad \Gamma_{\rm w}(r=0) = 0, \quad \frac{{\rm d}V}{{\rm d}r}(r=0) = 0.$$

3. Results and discussion

In this section, the calculation results obtained with a two-dimensional fluid model are presented, mainly discussing the effect of variations of the critical parameters on the deposition process of silicon nitride. A mixture of silane diluted in ammonia and nitrogen was used as a deposition precursor in this simulation. We did simulations for an arbitrary configuration of a capacitively coupled PECVD reactor (Fig. 1), where the discharge gap was $z2 - z1 = 2.0$ cm, two electrode radius $r1 = 16$ cm, $r1 - r2 = 12$ cm. The simulated reactor was driven by a 13.56-MHz radio frequency sinusoidal voltage. The amplitude of the potential was assumed to be $V_0 = 60$ V. The total pressure of background gases was $P_{\rm tot} = 1.5$ Torr (1 Torr = 1.3322×10^2 Pa), in which the gas pressure ratio of (N_2+NH_3) : SiH_4 = 19 : 1, and N_2 : NH_3 = 8 : 11. The temperatures of ions and background gases in our model were kept constant as $T_{\rm gas} = T_{\rm ion} = 400$ K. These parameters were kept at the above values, unless the gas pressure, the N_2/NH_3 ratio and the discharge gap. One RF cycle was divided into 2000 time-steps in all simulations. The discussion given below is based on the convergence of the fluid model, which ensures that the relative changes of the discharge parameters between two succeeding RF cycles are less than 10^{-6}.

Figures 2 and 3 show the spatial variation profiles of the electron number density $n_{\rm e}$ and the electron temperature $T_{\rm e}$ at the discharge conditions described above, respectively. It can be seen from Fig. 2 that the electron density presents a relatively high concentration in the bulk of the discharge, especially near the side of the electrode compared with those in the center, showing evidently the electrostatic edge effect. The plasma between the electrodes probably exists by diffusion inwards from the outside. Different from the traditional cylindrical chamber, a prominent diffusion is found in the discharge region. Moreover, due to the difference in the radius of two electrodes, the extra part of the upper one, i.e., the $r2$ region, the electron density can diffuse to the upper plate quickly. This effect can be attributed to a larger electron temperature near the upper plate, as shown in Fig. 3. It can also be observed from Fig. 3 that the electron temperature presents relatively high concentration in the gap which is between the electrodes' outer edge and the external ground electrode, suggesting that all the RF power is dissipated in the gap. Meanwhile, the electron temperature shows little fluctuation in the plasma region, but begins to oscillate obviously near the sheath region, under the influence of the RF source.

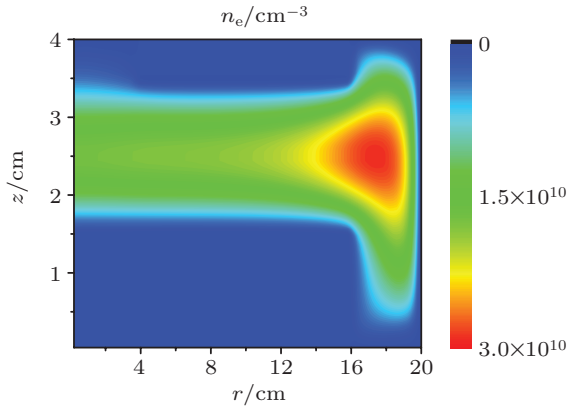


Fig. 2. (color online) The spatial variation profiles of the electron density $n_{\rm e}$, with (N_2+NH_3) : SiH_4 = 19 : 1, N_2 : NH_3 = 8 : 11, $P = 1.5$ Torr, $T_{\rm gas} = 400$ K, $V_0 = 60$ V, $f = 13.56$ MHz.

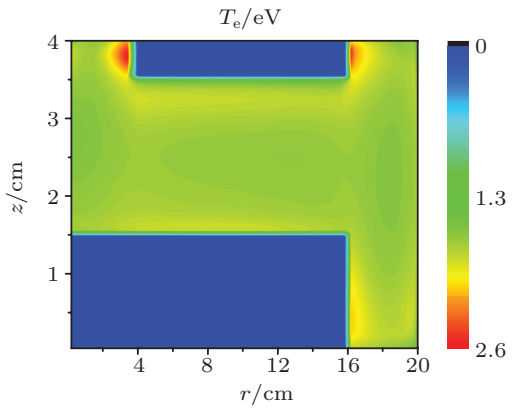


Fig. 3. (color online) The spatial variation profiles of the electron temperature $T_{\rm e}$, with settings being the same as those in Fig. 2.

The calculated density profiles of the main positive ions in the PECVD chamber are demonstrated in Fig. 4. As we can see that there is an obvious off-axis peak near the side electrode for the positive ions density of SiH_3^+, NH_3^+, and N_2^+, which is similar to the spatial distribution of electron density. Note that the positive ion SiH_3^+ is presented at the highest density, and takes a value of about 1.4×10^{10} cm^{-3}. The N_2^+ density, at 5.8×10^9 cm^{-3}, is relatively low. This can be explained by the fact that N_2^+ is only produced by electron impact collisions on N_2 above 15.6 eV.

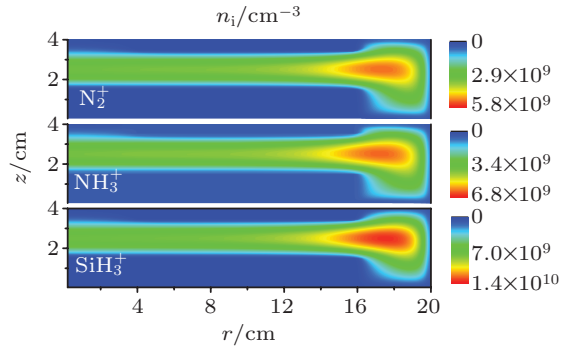


Fig. 4. (color online) The spatial variation profiles of the ion densities, with settings being the same as those in Fig. 2.

Comparing with ions, neutral radicals play an important part in the film growth. Thus, the spatial density profiles of main sticky radicals ($HSi(NH_2)$ and $H_2Si(NH_2)$, sticking coefficient 0.05) and a non-sticky radical (NH_2, sticking coefficient 0.0) are shown in Fig. 5. As we can see, the non-sticky profile shows an obvious edge-high distribution while the sticky radicals show a center-high distribution, implying that the main discharge region has moved from the side electrode region to the center between two electrodes with the increase of the sticking coefficient. Furthermore, according to the reactivity of the radicals with walls, the density of the sticky radicals decreases near the substrate. It should also be noted that $HSi(NH_2)$ and $H_2Si(NH_2)$ profiles reach a concentration of about 3.6×10^{14} cm^{-3} and 2.6×10^{14} cm^{-3} in the plasma bulk, respectively, which is approximately 20 times larger than NH_2, meaning that aminosilane radicals are the main deposition precursors in silicon nitride deposition. This conclusion is in agreement with the mass spectrometry analysis of Ref. [22].

As the gas pressure is one of the most easily controllable parameters in the plasma deposition processes. In Fig. 6, we present the spatial variation profiles of electron density at different pressures. We can see from Fig. 6 that the electron density increases definitely with the increase of the gas pressure. In the presence of a higher pressure, there will be a higher collision frequency. As a result, the collision between electrons and background neutrals becomes more frequent, and eventually there will be more electron impact dissociations, resulting in a higher electron density, as well as the radical density along the formation of deposition rate.

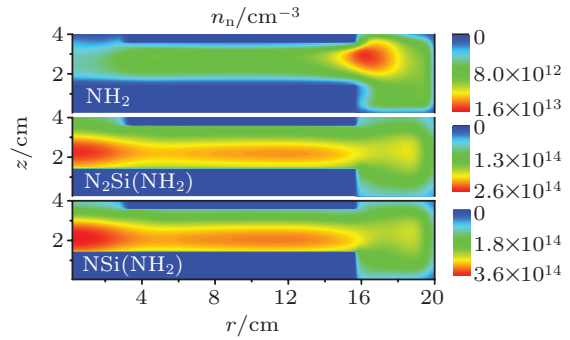


Fig. 5. (color online) The spatial variation profiles of the radial densities, with settings being the same as those in Fig. 2.

In order to illustrate the plasma uniformity variation with the process parameter, we introduce a non-uniformity degree α, which is defined as,[21,23]

$$\alpha = ((N_{\max} - N_{\min})/2N_{\text{av}})100\%, \tag{12}$$

where $N_{\max}$, $N_{\min}$, N_{av} represent the maximum, minimum, and average values of electron density, respectively. It can be observed in Fig. 6 that, at the pressure of 1.0 Torr, the electron density has poor uniformity over the bottom electrode. This is due to the fact that, when the gas pressure $P = 1.0$ Torr, and the RF power is mainly dissipated in the open region, thus a sudden increase of the electron density occurs at the edge of electrodes, resulting in poor uniformity. As the pressure increases, the non-uniformity degree α decreases from 34.4% to 7.7%. Which proves the effectiveness of the gas pressure control for improving the thin films' uniformity.

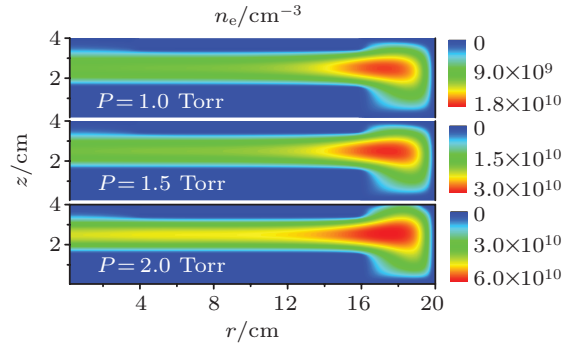


Fig. 6. (color online) The spatial variation profiles of the electron density n_e, with the gas pressure $P = 1.0$, 1.5, and 2.0 Torr, (N_2+NH_3) : $SiH_4 = 19 : 1$, $N_2 : NH_3 = 8 : 11$, $T_{\text{gas}} = 400$ K, $V_0 = 60$ V, $f = 13.56$ MHz.

For the silicon–nitride layer, the film characteristics depend strongly on the ratio of the process gases. Thus, the effects of N_2/NH_3 ratio on the electron density are investigated systematically in Fig. 7. It can be noticed in Fig. 7 that, upon increasing N_2/NH_3 ratio, the electron density decreases much slightly. This is due to the fact that there is no significant difference between the threshold energy of N_2 and NH_3. However, when N_2/NH_3 ratio increases from 6/13 to 10/9, the content of hydrogen decreased by 40%, which will finally cause a large decrease of hydrogen impurity. Thus, under the present conditions it seems that by properly selecting the ratio of the

process gases (NH_3 and N_2), the hydrogen impurity can be decreased significantly while a much smaller decrease in the plasma density can be achieved.

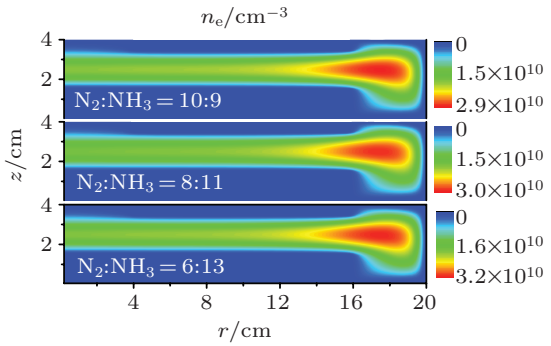


Fig. 7. (color online) The spatial variation profiles of the electron density n_e, with the gas pressure rate of N_2 : NH_3 = 6 : 13, N_2 : NH_3 = 8 : 11, and N_2 : NH_3 = 10 : 9, (N_2+NH_3) : SiH_4 = 19 : 1, P = 1.5 Torr, T_{gas} = 400 K, V_0 = 60 V, f = 13.56 MHz.

In order to clarify the discharge gap effect on the uniformity of plasma density in $SiH_4/N_2/NH_3$ discharges, the spatial variation profiles of electron density at different discharge gap are shown in Fig. 8. As seen from Fig. 8 that there is an obvious off-axis peak near the side electrode for the electron density at $z2-z1$ = 1.5 cm, while at $z2-z1$ = 3.0 cm the electron density profile shows a center-high. This is due to the fact that when the discharge gap $z2-z1$ = 1.5 cm, all the RF power is dissipated in the gap which is between the electrodes' outer edge and the external ground electrode. Hence, it is expected that the plasma density is highest at the edge of electrodes. When the discharge gap $z2-z1$ = 3.0 cm, the RF power is dissipated principally between the electrodes, hence the plasma is more uniform between the electrodes. Therefore, the uniformity of thin-film deposition can be well improved by controlling the discharge gap.

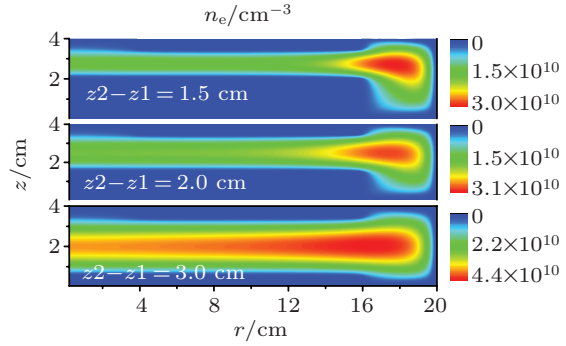


Fig. 8. (color online) The spatial variation profiles of the electron density n_e, with the electrode thickness $z2-z1$ = 1.5, 2.0, 3.0 cm, N_2 : NH_3 = 8 : 11, (N_2+NH_3) : SiH_4 = 19 : 1, P = 1.5 Torr, T_{gas} = 400 K, V_0 = 60 V, f = 13.56 MHz.

4. Concluding remarks

In summary, by using a two-dimensional fluid model, the properties of SiH_4, N_2, and NH_3 mixture plasmas driven by radio frequency voltage are investigated in a capacitively coupled arbitrary configuration PECVD reactor. The model includes 32 different species and the plasma dynamics equations, as well as chemical reactions are taken into accounted. In this work, we investigate in particular the influence of variations in process parameters, such as gas pressure, N_2/NH_3 ratio, and discharge gap, on the uniformity of electron density. A strong dependence of the plasma properties on the gas pressure and the discharge gap is shown. It has been concluded that the uniformity of plasma density are gradually improved with the increases of gas pressure and discharge gap.

From the standard model, it is found that the content of H can be decreased significantly, while the plasma density decreases slightly when N_2/NH_3 ratio increases. This implies that properly increasing the N_2/NH_3 ratio can be useful to achieve higher-quality film. Thus, the plasma parameters are more adjustable under an arbitrary configuration of radio-frequency CCP reactor, and these variations are conducive to providing better conditions for material processing and thin-film deposition.

References

[1] Sleeck E, Schaekers M, Shi X, Kunnen E, Degroote B, Jurczak M, de Potter, de ten Broeck M and Augendre E 2005 *Microelectron. Reliab.* **45** 865
[2] Liu X M, Song Y H and Wang Y N 2011 *Chin. Phys. B* **20** 065205
[3] Olson J M 2002 *Mater. Sci. Semicond. Process.* **5** 51
[4] Kubacki R M, Ionic Syst and Salinas C A 1995 *IEEE. Trans. Compon. Packag. Manuf. Technol.* **18** 471
[5] Lieberman M A and Lichtenberg A J 2005 *Principles of Plasma Discharges and Materials Processing*, 2nd edn. (New York: Wiley-Interscience)
[6] Sze S M 1985 *Semiconductor Devices: Physics and Technology* (New York: Wiley)
[7] Smith D L, Alimonda A S, Chen C C, Ready S E and Wacker B 1990 *J. Electrochem. Soc.* **137** 614
[8] Ray S K, Das S, Maiti C K, Lahiri S K and Chakraborti N B 1994 *J. Appl. Phys.* **75** 8145
[9] Kushner M J 1992 *J. Appl. Phys.* **71** 4173
[10] Ohta H, Nagashima A, Hori M and Goto T 2001 *J. Appl. Phys.* **89** 5083
[11] Nowling G R, Babayan S E, Jankovic V and Hicks R F 2002 *Plasma Sources Sci. Technol.* **11** 97
[12] Bavafa M, Ilati H and Rashidian B 2008 *Semicond. Sci. Technol.* **23** 095023
[13] De Bleecker K, Bogaerts A, Gijbels R and Goedheer W 2004 *Phys. Rev. E* **69** 056409
[14] Nienhuis G J, Goedheer W J, Hamers E A G, van Sark W G J H M and Bezemer J 1997 *J. Appl. Phys.* **82** 2060
[15] Fridman A A, Boufendi L, Hbid T, Potapkin B V and Bouchoule A 1996 *J. Appl. Phys.* **79** 1303
[16] Dollet A, Couderc J P and Despax B 1995 *Plasma Sources Sci. Technol.* **4** 94
[17] De Bleecker K, Herrebout D, Bogaerts A, Gijbels R and Descamps P 2003 *J. Phys. D: Appl. Phys.* **36** 1826
[18] Hayashi M 1987 *Swarm Studies and Inelastic Electron–Molecule Collisions*, eds. Pitchford L C, McKay V B, Chutjian A and Trajmar S (New York: Springer) pp. 167–190
[19] Perrin J, Leroy O and Bordage M C 1996 *Plasma Phys.* **36** 3
[20] McDaniel E W and Mason E A 1973 *The Mobility and Diffusion of Ions in Gases* (New York: Wiley)
[21] Liu X M, Song Y H, Xu X and Wang Y N 2011 *Phys. Plasmas* **18** 083508
[22] Smith D L, Alimonda A S, Chen C C, Ready S E and Wacker B 1990 *J. Electrochem. Soc.* **137** 614
[23] Volynets V, Shin H, Kang D and Sung D 2010 *J. Phys. D: Appl. Phys.* **43** 085203